

Solid-State Actuation of Rotor Blade Servo-Flap for Active Vibration Control

VICTOR GIURGIUTIU, CRAIG A. ROGERS AND RAZVAN RUSOVICI

Center for Intelligent Material Systems and Structures, Virginia Polytechnic Institute and State University, Blacksburg, VA 24061-0261

ABSTRACT: The basic concepts and some innovative ideas associated with the analysis, design, and experimentation of induced-strain actuators for rotor blade aeroelastic vibration control are presented and discussed. A trailing-edge servo-flap actuated by a hydraulically-amplified large-displacement induced-strain actuator is considered. Design requirements based on extensive literature review are proposed and utilized. The principle of high-power induced-strain actuation, and the energy and energy-density of several commercially-available induced-strain actuators are presented. A full-scale proof-of-concept demonstrator, designation HAHDIS Mk. 1, was designed, built, and tested. Results from static and dynamic tests are presented and discussed. Good frequency response of the full-scale proof-of-concept demonstrator was proven in the range of 1 to 30 Hz in spite of the power and current limitations of the available electronic equipment.

DESIGN REQUIREMENTS FOR INDUCED-STRAIN ACTUATED ROTOR BLADE ACTIVE CONTROL

ROTOR blade vibration reduction based on higher harmonic control—individual blade control (HHC-IBC) principles is a very attractive area of application for induced-strain actuators (ISA). Giurgiutiu et al. (1995a), recently reviewed the theoretical and experimental state of the art in achieving HHC-IBC through conventional and ISA methods. Several concepts were investigated (Millott and Friedmann, 1992; Librescu, Rogers and Song, 1992; Song and Librescu, 1993; Ben-Zeev and Chopra, 1995; Hall and Prechtel, 1995; Straub and Merkley, 1995). The servo-flap principle appeared to offer the most promising avenue for short-term implementation (Figure 1). It was found that the specialized literature proposed several servo-flap proposals, with different geometric configurations and aerodynamic characteristics, resulting in different ratios between flap and blade areas, chords, and spans. Although the force-displacement and moment-angle estimates for these varied flap geometries were found to differ significantly, a common-base could be identified in the peak energy requirements. Hence, a benchmark specification for a tentative HHC-IBC device based on the aerodynamic servo-flap principle using ISA could be developed.

The resulting benchmark values for peak energy, force-displacement product, and power are given in Table 1 along with other relevant parameters. For practical applications, it was found that an induced-strain actuator system capable of delivering a ± 1 mm stroke simultaneously with a ± 2.5 kN

force would provide the energy required of 1.25 J per blade necessary to implement the servo-flap principle. For increased reliability, a multi-segment servo-flap would be preferred, while the actuator requirement for each segment would be proportionately reduced. For example, a 2-segment flap would require 2 separate actuators of ± 1 mm stroke and ± 1.25 kN force.

Another important aspect that had to be addressed is that of the ceramic nature of most ISA stacks that makes them inherently weak in tension. Hence, the technical solution of having two directly-opposed stacks without tension connection was adopted. A schematic drawing of such an arrangement for producing the dynamic motion of an active servo-flap for rotor blade aeroelastic vibration control is shown in Figure 2. Analysis of the related implementation issues (Giurgiutiu et al., 1995a) produced useful results. First design iteration showed that direct actuation via long ISA stacks, though apparently simple, would not offer a feasible solution for actual implementation. The very large length required to produce the required ± 1 mm stroke would lead to excessive compressibility effects resulting in large displacement loss and parasitic internal strain energy. The second design iteration indicated that indirect actuation, using a generic displacement amplifier, would be much more feasible and even desirable since, in this way, the internal and external stiffness values could be efficiently matched. The optimal amplification gain was calculated using a closed-form formulation that relates the closed-loop amplification ratio to the stiffness ratio. These preliminary design studies shows that commercially available ISA stacks, coupled with an optimally-constructed displacement amplifier, are able to meet the benchmark force, stroke, and energy requirements.

This paper was originally presented at ICAST '95, November 13–15, 1995, Key West, Florida.

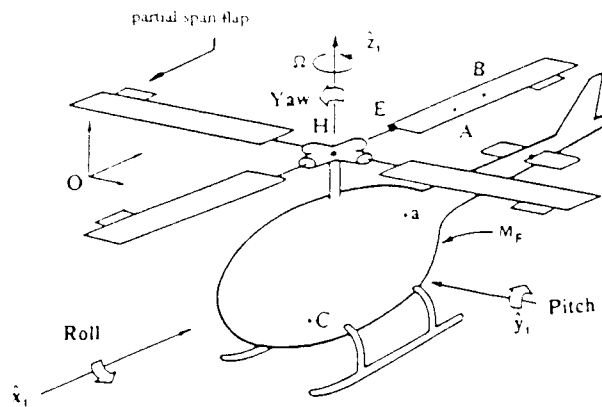


Figure 1. Rotor blade servo-flap principle for aeroelastic vibration control (Millot and Friedmann, 1992).

BASIC ASPECTS OF INDUCED-STRAIN ACTUATORS BASED ON ELECTROACTIVE AND MAGNETOACTIVE MATERIALS

Active materials exhibit induced-strain actuation (ISA)* under the action of an electric or magnetic field. Several active materials formulations have been developed in recent years. They are primarily of three types:

- PZT-Lead Zirconate Titanate—A ferroelectric ceramic material with piezoelectric properties and reciprocal behavior that converts electrical energy into mechanical energy and vice-versa. It accepts some amount of reversed poling thus achieving maximum contraction strokes of up to 25%–30% of the maximum expansion stroke. A vari-

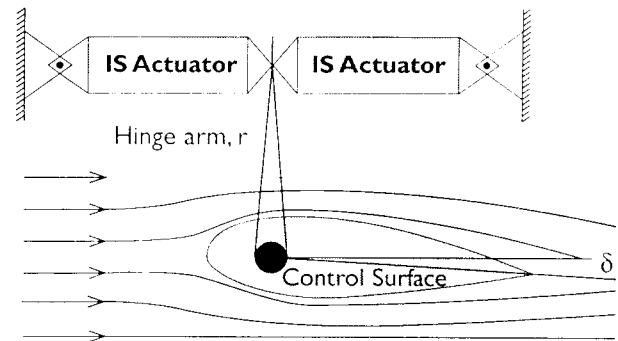


Figure 2. Schematic drawing showing the use of strain actuators to produce dynamic motion of an active servo-flap.

ety of PZT formulations have been developed to suit a wide range of frequency and amplitude requirements. PZT-5 is one of the most widely used formulations for actuator applications.

- PMN—Lead Magnesium Niobate—An electrostrictive ceramic material which, when suitably poled, displays piezoelectric-like properties and reciprocal behavior that converts electrical energy into mechanical energy and vice-versa. However, it does not display contraction under reversed poling. Numerous PMN formulations have been developed to suit a wide range of frequency and amplitude requirements.
- TERFENOL—TER (Terbium) FE (Iron) NOL (Naval Ordnance Laboratory)—A magnetostrictive alloy consisting primarily of terbium, dysprosium, and iron. Various TERFENOL formulations have been developed, as, for example, TERFENOL-D.

Table 1. General design requirements for an active servo-flap to produce aeroelastic vibration control of a typical helicopter rotor blade.

Parameter	Value and Units	Notes
Flap deflection	$\pm 1/30$ rad ($\approx \pm 2^\circ$)	
Hinge moment	± 75 Nm	Simultaneous with flap deflection
Frequency	25–30 Hz	
Maximum instantaneous energy transmitted to the airstream	1.25 J/blade	(Zero steady force is assumed)
Maximum instantaneous power transmitted to the airstream	0.5 kW	
ISA actuator weight budget	10 kg/blade	$\approx 10\%$ of typical blade weight
ISA system weight budget (including power supply, lead wires, controls, etc.)	80 kg/4-blade helicopter	$\approx 1\%$ of typical helicopter weight
Overall power consumption budget	10–12 kW/4-blade helicopter	$\approx 1\%$ of typical rotor power
Specific transmitted energy	0.125 J/kg	
Specific transmitted power	25 W/kg	
Specific power consumption	≤ 140 W/kg	Including all losses

*Here, the acronym ISA is used to signify either an induced-strain actuator or the induced-strain actuation principle.

Construction of a PZT or PMN Stack Actuator

An electroactive solid-state stack actuator consists of many layers of electroactive material (PZT or PMN) alternatively connected to the positive and negative terminals of a high-voltage source (Figure 3). Such a PZT or PMN stack behaves like an electrical capacitor. When activated, the electroactive material expands and produces output displacement. Typical strains for electroactive materials are in the range of 750–1200 $\mu\text{m}/\text{m}$. The PZT or PMN stacks are manufactured by two methods. In the first method, the layers of active material and the electrodes are mechanically assembled and glued together using a structural adhesive. The adhesive layer stiffness is at least an order of magnitude lower than the stiffness of the ceramic. Special attention is given to maintaining very thin adhesive layers and thus minimize the loss in overall effective stiffness of the resulting stack. In the second method, the ceramic layers and the electrodes are assembled in the “green” state, then fired together (co-fired) and, possibly, subjected to a high isostatic pressure (HIP process) to increase density and eliminate voids. This process ensures a much stiffer final product and, hence, a better actuator performance. However, processing limitations, such as oven and press size, etc., limit the applicability of this process to other than small stacks.

The PZT and PMN stacks are surrounded by a protective polymeric or elastomeric wrapping. Lead wires protrude from the wrapping for electrical connection. Steel washers, one at each end, are also provided for distributing the load into the brittle ceramic material. When mounted in the application structure, these stacks must be handled with specialized knowledge. Protection from accidental impact damage must be provided. Adequate structural support and alignment are needed. Mechanical connection to the application structure must be such that tension stresses are not induced in the stack since the active ceramic material has very low tension strength. Hence, the load applied to the stack must always be compressive and perfectly centered. If tension loading is also expected, adequate pre-stressing must be provided through springs or other means.

Construction of a TERFENOL Actuator

A magnetoactive solid-state actuator consists of a TER-

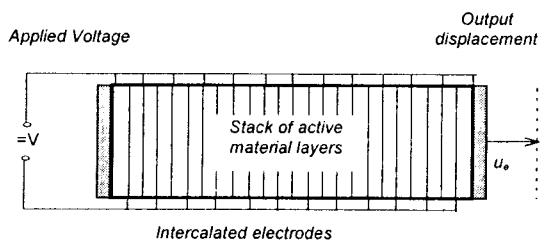


Figure 3. Induced strain actuator using a PZT or PMN electroactive stack.

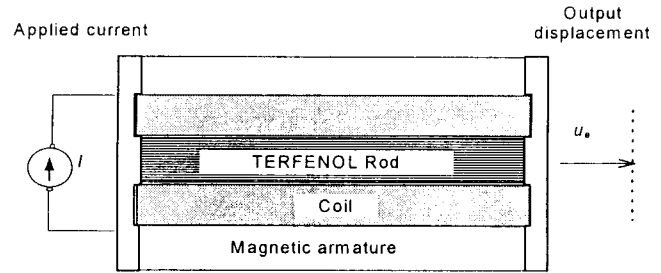


Figure 4. Induced-strain actuator using a TERFENOL magnetoactive rod.

FENOL bar inside an electric coil and enclosed in an annular magnetic armature (Figure 4). When the coil is activated, the TERFENOL expands and produces output displacement. The TERFENOL material has been shown to be capable of strains up to 2000 $\mu\text{m}/\text{m}$, but with high nonlinear and hysteresis penalties. Practical strains employed by the manufacturers of TERFENOL actuators are in the range of 750–1000 $\mu\text{m}/\text{m}$. The TERFENOL-D bar, the coil, and the magnetic armature are assembled between two steel-washers and put inside a protective wrapping to form the basic magnetoactive induced-strain actuator.

Performance of Solid-State Induced-Strain Actuator

Solid-state induced-strain actuators of various material types and different operation principles can be compared using two overall performance parameters:

- induced-strain actuation displacement, u_{ISA} , measured in mm
- internal stiffness, k_i , measured in kN/mm or N/mm

The induced-strain actuator displacement, u_{ISA} , is the result of the induced-strain effect, which is the basic property of the active material. Figure 5 shows a schematic drawing of an induced-strain actuator under two loading conditions: (a) a generic external force, $F = F(u_e)$, $F(0) = 0$, and (b) an external spring k_e .

The external load, $F(u_e)$, produces a backwards elastic displacement, $F(u_e)/k_i$, due to the compressibility of the actuator. Hence, the actuator output displacement, u_e , under load, $F(u_e)$, is given by:

$$u_e = u_{ISA} - \frac{F(u_e)}{k_i} \quad (1)$$

If the external reaction load, $F(u_e)$, varies linearly with the output displacement, u_e , one can assume an external spring, k_e , as shown in Figure 5(b). Thus:

$$F(u_e) = k_e \cdot u_e \quad (2)$$

After substitution and simplification, one gets an expression

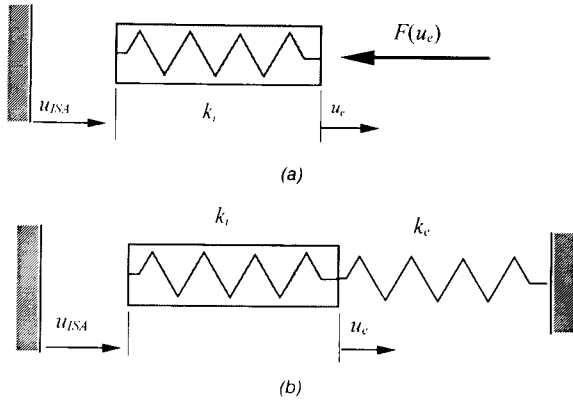


Figure 5. Schematic design of an induced-strain actuator: (a) under an external load $F(u_e)$, $F(0) = 0$; (b) under an external spring k_e .

for the output displacement, u_e , in terms of the stiffness ratio, $r = k_e/k_i$, i.e.,

$$u_e = \frac{1}{1+r} u_{ISA} \quad (3)$$

Output Energy of an Induced-Strain Actuator

Under quasi-static conditions, the output energy is:

$$E_e = \frac{1}{2} k_e \cdot u_e^2 \quad (4)$$

Substitution of Equation (3) into (4) yields the expression of output energy in terms of stiffness ratio, r :

$$E_e(r) = \frac{r}{(1+r)^2} \left(\frac{1}{2} k_i u_{ISA}^2 \right) \quad (5)$$

A plot of the output energy coefficient $E'_e(r)$, which signifies the variable part of Equation (5), is given in Figure 6. The function $E'_e(r)$ is zero for $r = 0$ ("free" condition)

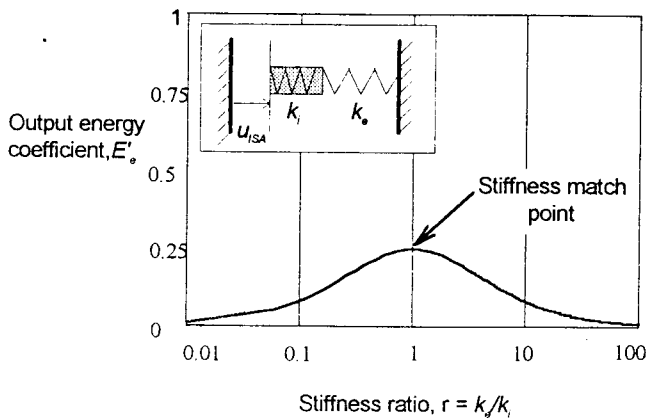


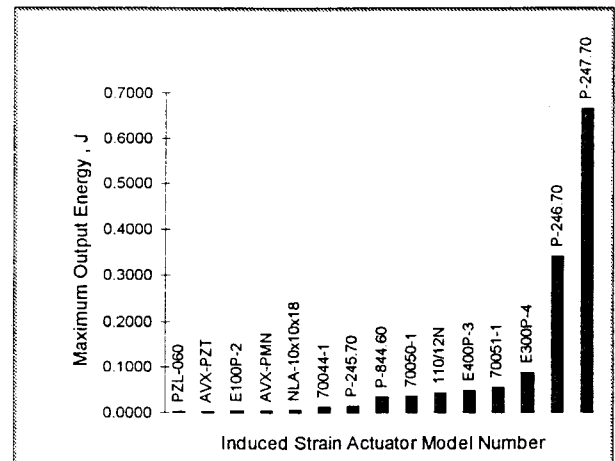
Figure 6. Stiffness match principle for peak energy delivery from an induced-strain actuator.

and $r \rightarrow \infty$ ("blocked" condition), and it has a maximum at $r = 1$. The $r = 1$ condition, with $k_e = k_i$, is called "stiffness match", (Giurgiutiu, Chaudhry and Rogers, 1995b), and identifies the maximum value of the output energy that can be delivered by an induced-strain actuator:

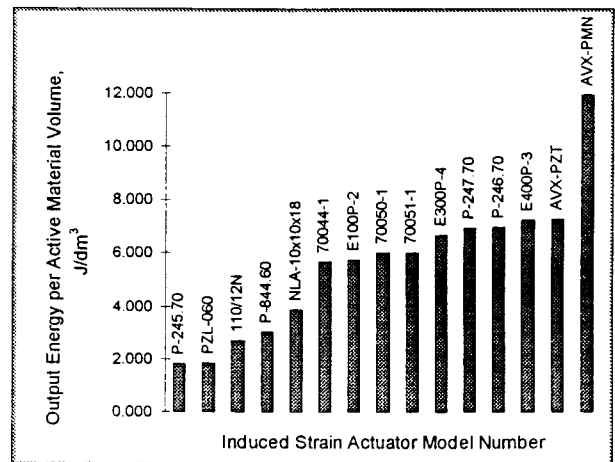
$$E_{emax} = \frac{1}{4} \left(\frac{1}{2} k_i u_{ISA}^2 \right) \quad (6)$$

Output Energy and Energy Density Comparison of Induced-Strain Actuators

Figure 7(a) shows a plot of output energy capabilities of various commercially-available induced-strain actuators of different sizes and operating principles. In order to attain a meaningful performance comparison, allowance for differences in volume and mass must be made. Dividing the actuator output energy by the actuator volume, one gets the volume-based output energy density [Figure 7(b)]. Similar



(a)



(b)

Figure 7. Performance comparison for fifteen commercially-available induced-strain actuators: (a) output energy; (b) volume-based output energy density.

calculations made in terms of mass and cost give a complete perspective of the induced-strain actuators' performance for application in rotor blade solid actuation design (Giurgiutiu, Ghaudhry and Rogers, 1996a).

HAHDIS SERIES ACTUATORS FOR ROTOR BLADE ACTIVE SERVO-FLAP CONTROL

The output displacement of present-day solid-state induced-strain actuators does not exceed the order of 0.1 mm. To use such a small output in actual rotor blade servo-flap actuation, some means of displacement amplification is necessary. After considering several options, we found that the hydraulic amplification principle offers attractive opportunities.

A device based on the hydraulic amplification principle can achieve large output displacements, while satisfying the stiffness and irreversibility requirements for aeroelastic control. A device based on the hydraulic amplification principle also offers versatility for rotor blade installation, since the induced-strain hydraulic drive and the hydraulic output actuator can be connected through conventional hydraulic lines, and can be placed in different locations inside the blade section to accommodate the geometric constraints. In our vision, such an induced-strain actuation system, based on hydrostatic principles, would be a self-contained sealed module, independent from the main aircraft hydraulic system.

To test the viability of our analysis, a full-scale proof-of-concept demonstrator, called a "Hydraulically Amplified High Displacement Induced-Strain" (HAHDIS) actuator, was designed and built in the Center for Intelligent Material Systems and Structures (CIMSS) at Virginia Tech (Figure 8). The HAHDIS proof-of-concept demonstrator was configured around a pair of high-power ISA devices with large free

strain displacement, $u_{ISA} = 0.120$ mm, and internal stiffness $k_i = 370$ kN/mm, capable of delivering a maximum output energy, $E_e = 0.666$ J. To produce an output resistance to the actuator and to simulate real-life external stiffness, a load simulator was also designed and built. The load simulator consisted of a double-leaf spring connected to a movable airfoil. The linear displacement of the HAHDIS actuator was transformed in angular displacement through a hinge arm of 28 mm. This arrangement was designed to produce an angular motion of around $\pm 2^\circ$, satisfying the initial requirements for an aeroelastic vibration control application.

TESTING OF THE HAHDIS ACTUATOR

Testing of the improved HAHDIS actuator is currently underway in CIMSS laboratory. The HAHDIS actuator was fully instrumented with force, displacement, and pressure transducers, and was subjected to static and dynamic tests. In the static tests, ISA input to the actuator was simulated by the turning of screws placed on dummy ISA devices. The predicted behavior was observed. Angle output measurements of $\pm 2^\circ$ were obtained with $\pm 1/4$ turn of a 3/8-24 UNF screw. These results confirmed the soundness of our design, and its capability for full scale applications. However, these initial tests showed some displacement losses even under no-load condition. Giurgiutiu et al. (1995a) discussed these displacement losses and identified the cause of their under the no-load conditions. It was found that high Coulomb friction between the piston seals and the cylinder bore was extremely detrimental to the proper operation of the device, and could produce up to 12.5% loss in the amplification ratio under the no-load test condition. The frictional losses were found to be especially important in the output cylinder, due to the inverse-lever-arm effect of the amplification device.

In the improved HAHDIS design, the frictional losses in

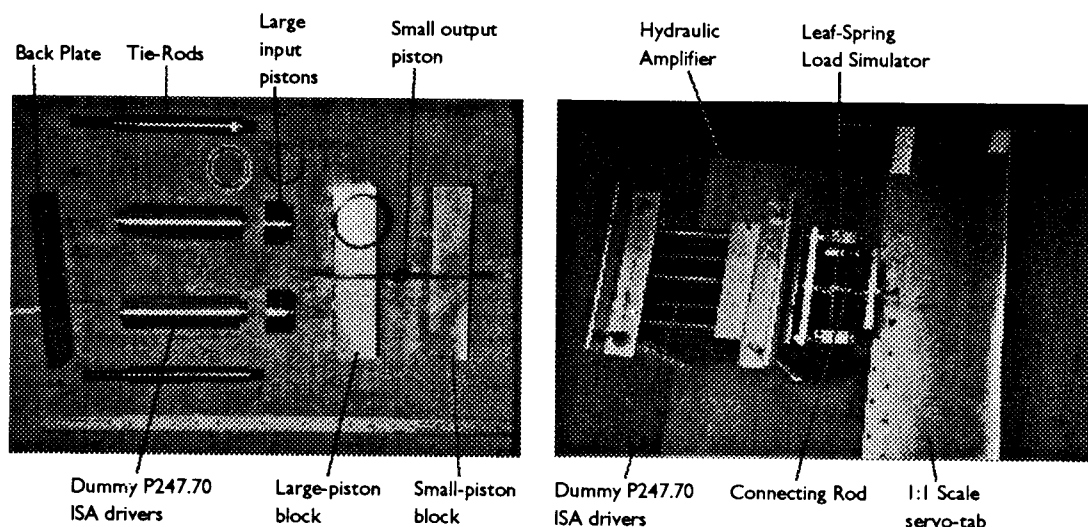


Figure 8. Layout and internal construction of the hydraulically-amplified high-displacement induced-strain (HAHDIS) actuator.

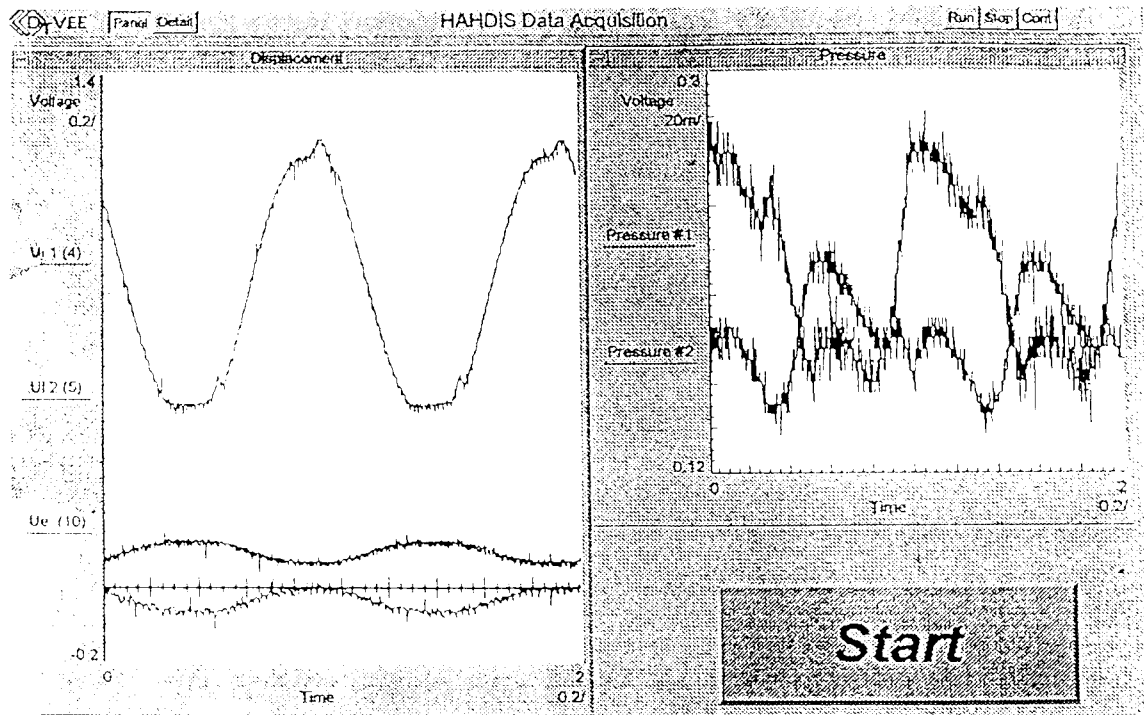


Figure 9. Input and output displacement data captured over a two-second duration at 1 Hz.

the output cylinder were reduced to very low values. These improvements were achieved through the use of a "labyrinth" type output piston instead of the conventional rubber-seal piston. This design eliminated friction between the piston seals and the cylinder bore, while preserving the fluid pressure under dynamic condition through the dynamic sealing effect of the labyrinth construction. The amplification ratio of the improved HAHDIS actuator under no-load condition and quasi-static operation was found to be very close to the design value of 16:1. To eliminate the residual air bubbles, introduced during the charging of the HAHDIS actuator with hydraulic, were eliminated through a specially designed bleed valve system. The loading and repressurization of the system was easily achieved with readily available hydraulic equipment, such as a hand pump.

For dynamic testing, four E300-P4 PMN stacks acquired from EDO Corp. were used. These actuators were stacked into pairs and installed at the reciprocal-acting input cylinders of the HAHDIS device. The PMN stacks were energized with a pair of high-voltage sinusoidal signals (400 ± 400 V) produced by a dual-channel model 50/750 TREK high-voltage amplifier. The two signals are in opposite phase, though maintaining the same bias off-set. This arrangement permits one stack to expand, while the other retreats. The hydraulic fluid is sent back-and-forth to the "in" and "out" chambers of the output cylinder, thus producing an alternating motion. During dynamic tests, a range of discrete frequencies between 1 Hz and 30 Hz, was sampled. The series of discrete frequencies started at 1 Hz and went up to 30 Hz, through increments of 1 Hz. At each frequency, data collec-

tion was done with the VTDEE software using a sampling rate of 100 Hz. The data was stored in the computer memory into an MS-EXCEL 5.0 file. For quick reference, captures and print-outs of the data screen were also performed. The sampled data consisted of the input and output displacements, u_i , u_o , and u_e , and of the pressures in the two chambers, p_1 and p_2 . Figure 9 presents an example of the displacement and pressure data captured at 1 Hz over the two-second time period. The resulting high displacement amplification effect is clearly illustrated: the small input displacement signals shown at the bottom of the graph are amplified into the very large output signal shown in the upper portion of the graph.

It should be noted that the same displacement calibration factor of 1.3089 mm/V applies for all the displacement traces. The pressure data in the two chambers is shown in the left portion of Figure 9. The anti-phase characteristics of the pressure waves are apparent. The pressure calibration factor was 200 psi/V. The pressure in the hydraulic chambers #1 and #2 has static-bias components of 292 psi and 331 psi, and dynamic components of 78 psi and 95 psi, respectively. The fact that the dynamic components of the hydraulic pressures are similar in magnitude and of opposite phase illustrates the satisfactory operation of the device. Figure 10 presents an example of the displacement and pressure data captured at 10 Hz over a two-second time period and shows the result of the high displacement amplification, as well as the clear reduction in input displacement due to limitations of the power supply. It is noted that the input displacements have decreased considerably due to the 50 mA current limitations of the model 50/750 TREK high-voltage power amplifier.

However, the effect of the displacement amplification is clearly illustrated: the very small input displacement signals shown at the bottom of the graph are amplified into the very large output signal shown in the upper portion of the graph. At 10 Hz frequency, the displacement amplification ratio was found to be approximately 15.3 times, which is very close to the design value of sixteen times.

It is believed that this good response is partly due to the beneficial effect from a possible external system resonance, which clearly reduces the effective output load. However, the stable and controllable behavior of the device under resonance conditions is an added merit of the HAHDIS concept. Figure 11 presents an example of the displacement and pressure data captured at 30 Hz over a two-second time period shows that the high displacement amplification can produce sizable output waveform from almost imperceptible input displacement. It is noted that, due to the 50 mA current limitations of the model 50/750 TREK high-voltage power amplifier, the input displacements have decreased very much, as shown at the bottom of the graph. However, due to the powerful displacement amplification, a sizable output displacement is still observed. This illustrates once again the benefits of the HAHDIS design concept. Figure 12(a) shows the frequency response curve for the no-load tests in the interval 1 to 30 Hz.

The output displacement response amplitude, u_e , has a moderate increase up to 10 Hz, and a decrease afterwards. Examination of the average input displacement curve, $u_{i\text{average}}$, shows that it is also decreasing. Additional examination of the oscilloscope data during the experiment showed

that the high-voltage signal provided by the model 50/750 TREK amplifier started to become angular below 10 Hz, indicating that the upper limit of the amplifier performance has been reached. Above 10 Hz, the amplifier signal deteriorated much faster, and its amplitude rapidly decreased. Thus, the decreased input voltage resulted in decreased input displacement to the device, and explains the observed decrease in output displacement amplitude. When we compensated for the loss of input displacement, the output displacement curve became almost flat [curve u_e^* in Figure 12(a)]. This proves the effectiveness of the HAHDIS principle, showing its good performance over the frequency range 1–30 Hz in spite of the input displacement decrease due to limitations in the high-voltage power supply. (The fact that the input displacements were not equal to the free stroke is attributed to the internal friction between the input pistons and the cylinder bores.)

The no-load results presented in Figure 12(a) constitute a considerable improvement from the results previously reported by Giurgiutiu et al. (1995a). The improvement is observed in the frequency range (50% increase from 20 to 30 Hz) and in the maximum peak-to-peak amplitude (50% increase from 0.8 to 1.2 mm). These improvements are mainly attributable to the reduction in the internal friction of the HAHDIS Mk. 1 actuator through improvement of the output piston.

In order to measure the performance of the improved HAHDIS Mk. 1a induced-strain actuator under actual load, a light realistic flap was connected at the actuator output. This flap was made from the rudder tab of a CESSNA light aircraft. The flap had a quadrilateral plan form of approx-

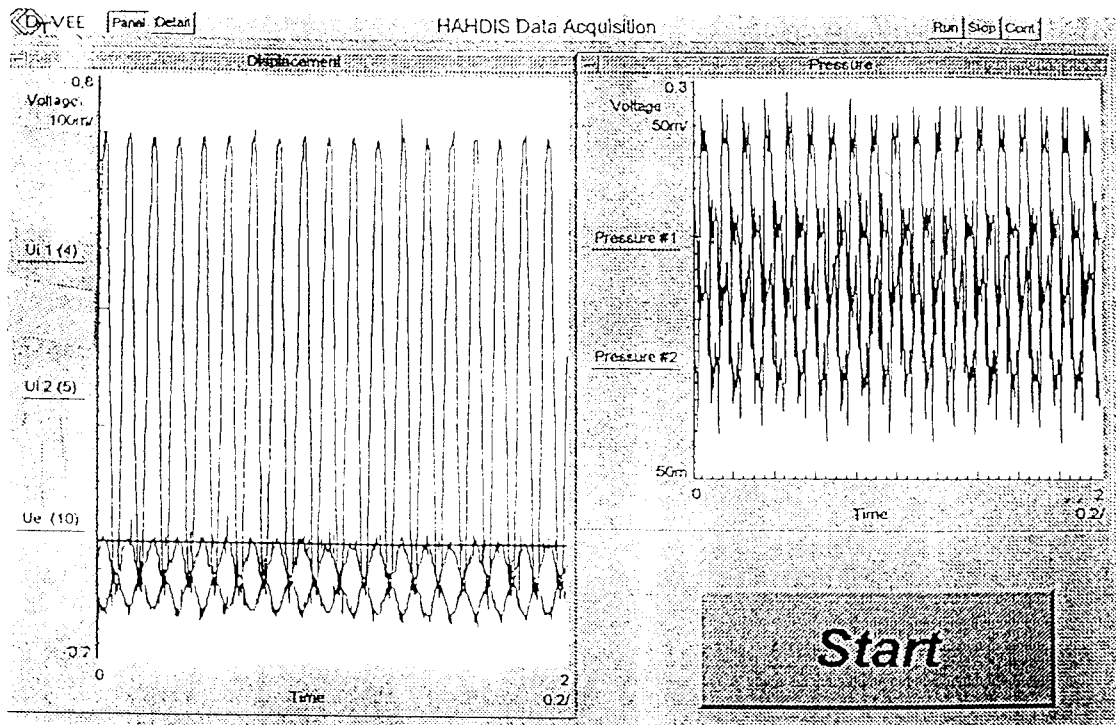


Figure 10. Input and output displacement data captured over a two-second duration at 10 Hz.

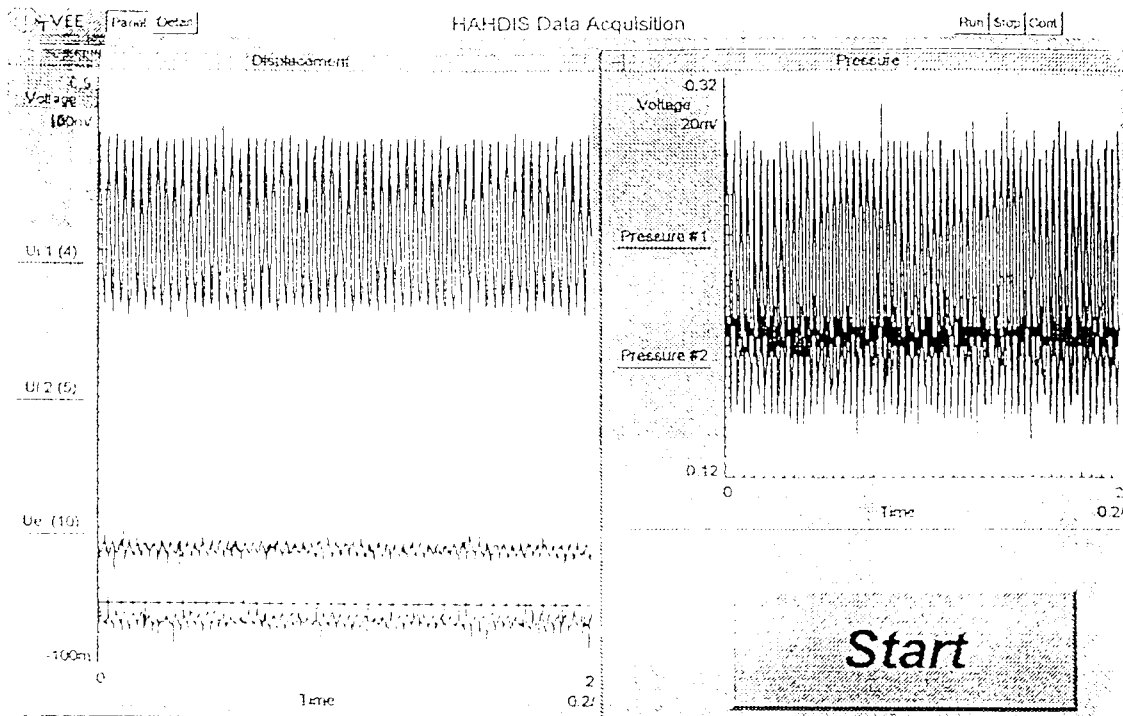


Figure 11. Input and output displacement data captured over a two-seconds at 30 Hz duration.

imately 480 mm × 140 mm (19 in × 5.5 in), and a weight of 0.420 kg (0.84 lb). The flap was operated over the same 1–30 Hz frequency range, and very good frequency response was noted throughout. The frequency response curve for the improved HAHDIS Mk. 1 induced-strain actuator under the inertial load provided by the realistic flap is shown in Figure 12(b).

Comparison of the HAHDIS Mk. 1 Dynamic Test Results

Table 2 presents an overview of the three HAHDIS Mk. 1 experiments indicating the maximum amplitude, the maximum frequency, and the limiting frequency due to the inadequacy of the electronic power amplifier resulting in a limited electrical supply to the ISA stacks. Comparative examination

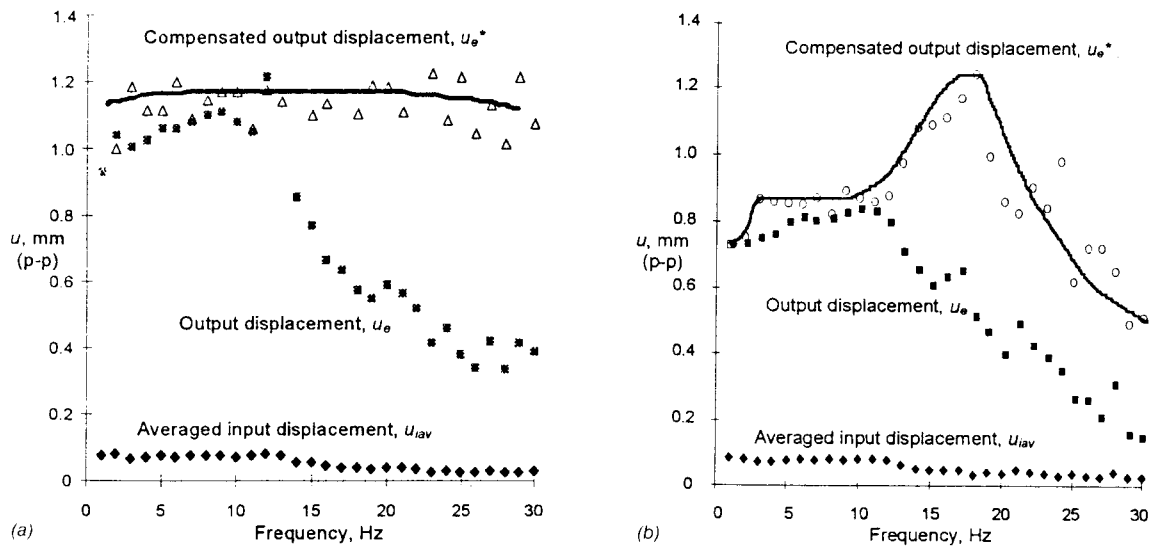


Figure 12. Frequency response curves of the improved HAHDIS Mk. 1a demonstrator in the range 1–30 Hz: (a) no external load; (b) low inertial from light realistic flap.

Table 2. Overview of the test results with the improved HAHDIS Mk. 1 actuator.

	Maximum Amplitude mm, p-p	Maximum Frequency Hz	Limiting Frequency Due to the Electrical Supply, Hz
Case 1: No-load	1.2 mm	> 30 Hz	10 Hz
Case 2: Realistic inertial load	1.25 mm	> 30 Hz	10 Hz
Case 3: Previous results (internal friction and heavy inertial load, Giurgiutiu et al., 1995a)	0.85 mm	20 Hz	5 Hz

of these results allows us to draw the following conclusions about the behavior of the induced-strain solid-state actuator under various load conditions when energized by a power supply with limited current delivery capabilities:

1. Under heavy inertial load and high internal friction (Case 3 in Table 2), the original HAHDIS Mk. 1 actuator showed an inadequate performance that was limited in both amplitude and maximum frequency. The amplitude limitation can be attributed to the internal compressibility and counter electro-motive force in the active-material stacks. The maximum frequency limitation is due to the limited capability of the power supply, since the current requirements are directly proportional with the stack capacitance and inversely proportional with frequency. In this heavy-load high-friction case, the current limitation was reached around 5 Hz.
2. Under no load (Case 2 in Table 1), the improved HAHDIS Mk. 1a actuator could easily achieve 30 Hz response with 1.2 mm p-p amplitude, which represent a 41% amplitude increase and a 50% frequency increase from Case 3. The increase in amplitude is attributed to the reduced compressibility loss and reduced counter electro-motive force in the stacks. The increase in range is explained by the decrease in stack admittance following the decrease in the inertial loads (phase angle $\phi = 180^\circ$). The electric current limitation of the power supply were reached around 10 Hz.
3. Under light inertial load (Case 1 in Table 1), the improved HAHDIS Mk. 1a actuator proved itself able to deliver at the required displacement over the required frequency range of 1 to 30 Hz. This infers that the HAHDIS Mk. 1a proof-of-concept demonstrator has fulfilled its purpose successfully, and has proven the feasibility of using induced-strain actuators to achieve realistic amplitudes over the frequency range required for active and adaptive control.

ROTOR BLADE IMPLEMENTATION OF THE HAHDIS CONCEPT

Figure 13 shows a proposal for the implementation of the HAHDIS Mk. 2 concept into an actual helicopter rotor blade. The sealed hydrostatic principle of modular design is adopted. The HAHDIS system consists of two main units

connected through short hydraulic pipes. The first unit is the solid-state hydraulic drive [Figure 13(a)]. It consists of two counter-acting active material stacks: each stack operates a separate hydraulic chamber. In order to minimize frictional losses, the hydraulic chambers contain deformable diaphragms instead of conventional pistons. The second unit consists of a rotary actuator mounted on the servo-flap [Figure 13(b)]. The two chambers of the rotary actuators are connected to the chambers of the hydraulic drive. Thus, the complete system is sealed and self contained. When stack #1 of the hydraulic drive is activated to expand, hydraulic fluid is sent forward to chamber #1 of the rotary actuator and produced an upward deflection of the flap. Simultaneously, stack #2 is activated to retreat, and thus accepts the excess fluid from chamber #2 of the rotary actuator into chamber #2 of the hydraulic drive. To produce the opposite effect, i.e., a downward motion of the flap, stack #2 is activated to expand, while stack #1 is activated to retreat. Through alternating expansion and retreat of the two stacks, an up-and-down motion of the flap is achieved.

The HAHDIS Mk. 2 concept is not fundamentally different from the HAHDIS Mk. 1 concept, only that its implementation solution has been adapted to fit inside the restricted space of a rotor blade or a wing. Additionally, by placing the main weight of the system, i.e., the hydraulic drive, in the leading edge of the aerodynamic section, the HAHDIS Mk. 2 concept ensures adequate mass balance as a prerequisite for flutter prevention. Remarkable about the HAHDIS Mk. 2 concept is its ability to attain high frequency response, since, unlike the conventional servo-valve-based systems, it is not based on hydraulic switching. Additionally, since the active material behavior is directly coupled with the airstream response, opportunities for reactive power recirculation can be explored.

CONCLUSION

The feasibility of solid-state actuation of helicopter servo-flap for rotor blade active control was studied theoretically and experimentally. The design requirements (force, displacement, and energy) for this application were identified. The capabilities of commercially available induced-strain actuators were reviewed and the energy feasibility of the induced-strain actuation was established. To achieve implementation of a large-displacement induced-strain actuator,

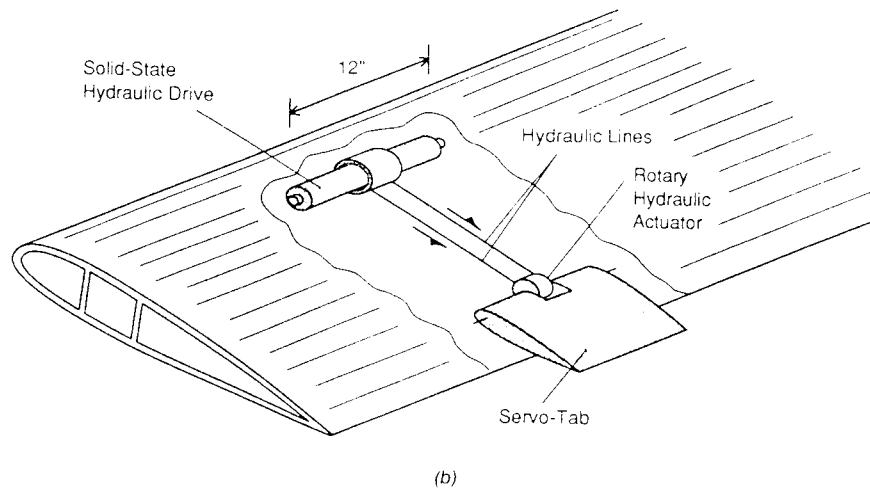
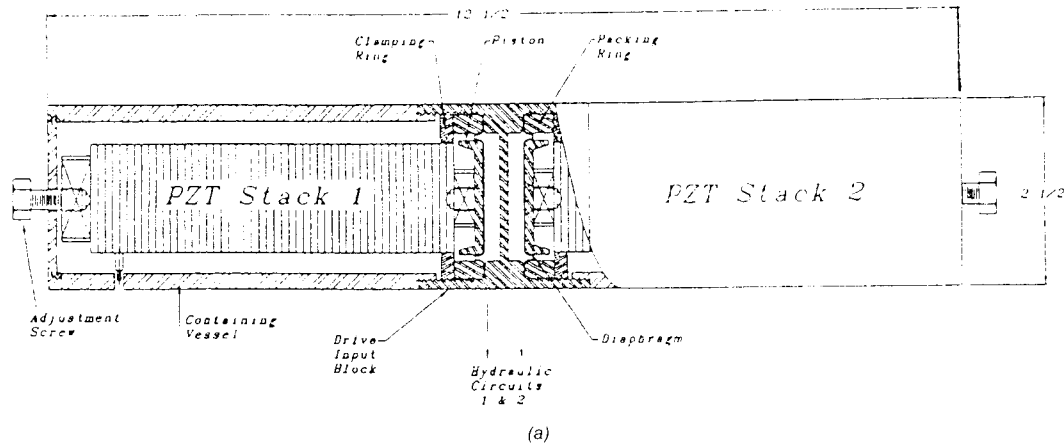


Figure 13. The proposed HAHDIS Mk. 2 solid-state actuator proposed for implementation in an actual helicopter rotor blade application: (a) the solid-state hydraulic drive; (b) the modular rotor blade implementation.

the hydrostatic amplification principles were adopted for experimental confirmation a full-size hydraulically-amplified high-displacement induced-strain (HAHDIS Mk. 1) proof-of-concept demonstrator was redesigned and built. The HAHDIS Mk. 1 demonstrator was subjected to static and dynamic testing in CIMSS laboratory. After initial testing, improvements of the HAHDIS Mk. 1 device were implemented to reduce the internal frictional losses. The improved HAHDIS Mk. 1a actuator was subjected to extensive dynamic testing in the 1 to 30 Hz frequency range. The no-load frequency response curve showed excellent behavior over the full frequency range, in spite of the power and current limitations of the electronic equipment. Further tests using a realistic inertial load were also performed, and fully proved the capability of the HAHDIS Mk. 1a actuator to achieve full flap actuation over the required frequency range. For in-flight implementation of the HAHDIS principle, a modular HAHDIS Mk. 2 conceptual design capable of installation within the restricted space and geometry of an actual helicopter blade has been proposed and discussed, and its potential benefits in terms of high frequency response and reactive power recirculation have been highlighted.

ACKNOWLEDGEMENTS

The authors gratefully acknowledge the support of the Army Research Office—University Research Initiative Program, Grant No. DAAL03-92-0181, Dr. Gary Anderson, Program Manager.

REFERENCES

- Ben-Zeev, O. and I. Chopra. 1995. "Development of an Improved Helicopter Rotor Model with Smart Trailing Edge Flaps for Vibration Suppression", *1995 SPIE North American Conference on Smart Structures and Materials, Smart Structures and Integrated Systems*, 26 February–3 March, San Diego, CA, Paper #2443-01 (in press).
- Giurgiutiu, V., Z. Chaudhry and C. A. Rogers. 1994. "The Analysis of Power Delivery Capability of Induced-Strain Actuators for Dynamic Applications", *Proceedings of the Second International Conference on Intelligent Materials, ICIM '94*, June 5–8, Colonial Williamsburg, VA: Technomic Pub. Co., Inc., pp. 565–576.
- Giurgiutiu, V., Z. Chaudhry and C. A. Rogers. 1995a. "Engineering Feasibility of Induced-Strain Actuators for Rotor Blade Active Vibration Control", *Journal of Intelligent Material Systems and Structures*, Technomic Pub. Co., September, 6(5):583–597.
- Giurgiutiu, V., Z. Chaudhry and C. A. Rogers. 1995b. "Stiffness Issues in the Design of ISA Displacement Amplification Devices: Case Study of a Hydraulic Displacement Amplifier", *Smart Structures and Materials '95*, San Diego, CA, 26 February–3 March, Paper #2443-12, SPIE Vol. 2443, pp. 105–119.
- Giurgiutiu, V., Z. Chaudhry and C. A. Rogers. 1995c. "Issues in the Design and Experimentation of Induced-Strain Actuators for Rotor Blade Aeroelastic Control", *Tenth VPI & SU Symposium on Structural Dynamics and Control*, May 8–10, Blacksburg, VA.
- Giurgiutiu, V., Z. Chaudhry and C. A. Rogers. 1996a. "Energy-Based Comparison of Solid-State Actuators", *Journal of Intelligent Material Systems and Structures*, Technomic Pub. Co., Inc., 7(1):4–14.
- Giurgiutiu, V., C. A. Rogers and R. Rusovici. 1996b. "Power and Energy Issues in the Induced-Strain Actuation for Aerospace Adaptive Control", *Proceedings of the 37th AIAA/ASME/AHS Adaptive Structures Forum*, Salt Lake City, UT, April 18–19, paper AIAA-96-1300-CP, pp. 301–311.
- Hall, S. R. and E. F. Prechtel. 1995. "Development of a Piezoelectric Servoflap for Helicopter Rotor Control", in *Active Materials and Smart Structure, Proceedings of the Symposium*, Texas A&M University, College Station, TX, October 10–12 (A95-23026 05-39), Bellingham, WA, SPIE Proceedings, Vol. 2427, pp. 16–19.
- Librescu, L., C. A. Rogers and O. Song. 1992. "Static and Dynamic Behavior of Adaptive Aircraft Wing Structures Modeled as Composite Thin-Walled Beams", *Proceedings of the 6th Japan-US Conference on Composite Materials*, Grosvenor Resort, Orlando, Florida, June 22–24, Technomic Pub. Co., Inc., pp. 713–724.
- Millott, T. A. and P. P. Friedmann. 1992. "Vibration Reduction in Helicopter Rotors Using an Active Control Surface Located on the Blade", *Proceedings of the AIAA/ASME/ASCE/AHS/ASC 33rd Structures, Structural Dynamics, and Materials Conference*, Dallas, TX, April, paper AIAA-92-2451-CP, pp. 1975–1988.
- Song, O. and L. Librescu. 1993. "Vibration Behavior of Rotating Helicopter Blades Incorporating Adaptive Capabilities", *Proceedings of SPIE 1993 North American Conference on Smart Structures and Materials*, Albuquerque, 1–4 Feb., pp. 354–365.
- Straub, F. K. and D. J. Merkley. 1995. "Design of a Smart Material Actuator for Rotor Control", *1995 SPIE North American Conference on Smart Structures and Materials, Smart Structures and Integrated Systems*, 26 February–3 March, San Diego, CA, Paper #2443-10, SPIE Vol. 2443, pp. 89–104.